Applied Catalysis B: Environmental 249 (2019) 266–274

Contents lists available at ScienceDirect

Applied Catalysis B: Environmental

journal homepage: www.elsevier.com/locate/apcatb

Defective borate-decorated polymer carbon nitride: Enhanced photocatalytic NO removal, synergy effect and reaction pathway

Jiwu Cao[a], Jingyuan Zhang[a], Xing'an Dong[a], Hailu Fu[c], Xianming Zhang[a], Xiaoshu Lv[a], Yuhan Li[a], Guangming Jiang[a,b,*]

[a] Engineering Research Center for Waste Oil Recovery Technology and Equipment, Ministry of Education, Chongqing Technology and Business University, Chongqing, 400067, China
[b] Institute of Fundamental and Frontier Sciences, University of Electronic Science and Technology of China, Chengdu, 611731, China
[c] Department of Environmental Engineering, China Jiliang University, Hangzhou, 310018, China

ARTICLE INFO

Keywords:
Carbon nitride
NO removal
Borate decoration
Photocatalysis
In situ DRIFTS

ABSTRACT

This work developed one effective approach to introduce both the N defect and borate group on polymer carbon nitride (PCN) by facilely immersing it in a $NaBH_4$ aqueous solution, and simultaneously control their number by varying the $NaBH_4$ concentration. The resultant defective borate-decorated PCN (denoted as X-B-PCN, X refers to the used $NaBH_4$ concentration) shows highly efficient in removing the ppb-level NO from an air flow under visible light irradiation. The removal efficiency displays a volcano-like variation with X, and the peak one reaches 44.1% by 1.32-B-PCN. The comparative studies on the optical property, the yield of active radicals, and the oxygen adsorption behaviors of PCN and X-B-PCN reveal that the synergy of N defect and borate decoration promotes the light absorbance, charge carrier separation and molecular oxygen adsorption, all of which contribute to an enhanced generation of the $^{\cdot}O_2^-$ and $^{\cdot}OH$ radicals for a better photocatalytic performance. The relative contribution of N defect to borate group in this synergy also depends on the X value, but the borate group always takes the major role. The *in-situ* DRIFTS investigation reveals that the NO is converted to nitrate. Overall, our work offered one viable strategy to make full use of the defect and group decoration for photocatalytic performance optimization of the PCN-based materials.

1. Introduction

Photocatalysis represents one highly promising technique for air pollution remediation due to its exceptional efficiency, green feature (using clean solar energy instead of chemicals) and low secondary pollution risk [1–3]. It initiates with the excitation of electron-hole pairs under solar light illumination, which then react with the surrounding molecular water and oxygen to generate oxidative radicals (such as $^{\cdot}OH$ and $^{\cdot}O_2^-$). These radicals are highly active and capable to mineralize/detoxify air pollutants (such as SO_x, NO_x, and volatile organic compounds) in a complete and rapid manner [4]. In the development of photocatalysis, the key task is to exploit economic, efficient and durable photocatalysts. Among various investigated ones, polymer carbon nitride (PCN) has received tremendous research interests due to its narrow band gap allowing the utilization of solar light, proper band edge energies for target reactions, and stable chemical structure [5–7]. However in practical applications, PCN still suffers from a poor light absorption and the rapid recombination of charge carriers, and usually performs unsatisfied [8–11].

To improve this situation, various strategies, including heterojunction construction [12–14], heteroatom doping [15–17], defect engineering [18–20] and surface modification [21–23], have been extremely exploited. Among them, the defect engineering on PCN has been widely accepted as one effective strategy, and has shown success in promoting the photocatalytic performance of PCN in various fields, such as H_2 production [24] and organic molecular mineralization [25]. It was reported that the introduction of the C or N defects can optimize the electronic band structure of PCN to promote light harvesting, and simultaneously serve as the electron sink to separate the charge carriers [26]. In spite of these merits, the defect application in the PCN-based photocatalysis is still limited by the harsh conditions for its synthesis/engineering. Currently, the defects in PCN were usually created by a solid-state thermal or hydrothermal polymerization process that is operated under a high temperature and a reductive atmosphere [27,28]. Such a process is usually accompanied with the high energy consumption, the large mass loss and the easy agglomeration of PCN layers.

* Corresponding author.
E-mail address: jiangguangming@zju.edu.cn (G. Jiang).

https://doi.org/10.1016/j.apcatb.2019.03.012
Received 13 December 2018; Received in revised form 14 February 2019; Accepted 2 March 2019
Available online 05 March 2019
0926-3373/

Therefore, it is highly desirable to explore one facile and efficient approach to prepare defective PCN.

The surface modification, especially by some acidic groups, such as SO_4^{2-} and PO_4^{3-}, has recently been verified to be highly effective to improve the activities of various photocatalysts, such as TiO_2 and PCN [29,30]. These acidic groups were claimed to intensify the O_2 adsorption on catalyst [31], and promote the utilization of hot electrons for an enhanced charge carrier separation and an enhanced generation of oxidative radicals [32,33]. The acidic group decoration was usually achieved by immersing the photocatalyst in an acidic group-contained aqueous solution, and actually no other alternative approach was reported [34].

Based on the above considerations, here we attempted to develop one promising PCN photocatalyst with the decoration of both the defect and acidic group (BO_3^{3-}) for the visible light-driven photocatalytic removal of ppb-level NO from the air. In searching of the synthetic methods, we were exciting to find that by immersing the PCN in a concentrated $NaBH_4$ aqueous solution at room temperature for 15 min, the dual decoration can be realized. It was demonstrated that $NaBH_4$ with a high reductive potential could etch the N atom off the PCN framework with itself converted to Na_3BO_3 and H_3BO_3, which were then adsorbed over the surface of PCN to achieve BO_3^{3-} group decoration. Based on this reaction mechanism, the number of both the N defect and borate can be facilely tuned by varying $NaBH_4$ concentration in solution. The overall contribution of N defect and borate as well as the separated contribution of each one to the optical property, charge carrier separation efficiency and the photocatalytic activity of PCN was then evaluated. The involved mechanism for the synergy of N defect and borate decoration was also investigated by a further identification of the generated active radicals and the O_2 adsorption behaviors on catalyst. Finally, the reaction pathway of the photocatalytic NO oxidation over the defective borate-decorated PCN was investigated by the *in situ* Diffuse Reflectance Infrared Fourier Transform Spectroscopy (DRIFTS) technique.

2. Experimental section

2.1. Material syntheses

Synthesis of PCN. In a typical synthesis [35], 20 mL of the urea aqueous solution (0.5 g mL^{-1}) was poured in an uncovered alumina crucible, and dried at 60 °C. The dried urea solid was sealed in the alumina crucible by a lid, and then calcined at 550 °C in muffle furnace. After a reaction of 2.0 h, light yellow PCN powders were obtained.

Preparation of the defective borate-decorated PCN. 0.25 g of the as-synthesized PCN was dispersed in 60 mL of deionized water. 15 mL of the $NaBH_4$ aqueous solution in different concentrations (0.13, 0.52, 0.92, 1.32, 1.98 and 2.64 M) was then dropwise added to the above dispersion. The mixture was kept vigorous stirring for another 15 min, then filtrated and washed with 50 mL of deionized water. The collected product was finally dried at 60 °C for further use. The untreated and $NaBH_4$-treated PCN were labeled as PCN and X-B-PCN (X = 0.13, 0.52, 0.92, 1.32, 1.98 and 2.64), respectively.

2.2. Characterization

The X-ray diffraction (XRD) pattern was measured on an X-ray diffractometer (model D/max RA, Rigaku Co., Japan) under the Cu Kα irradiation. The sample morphology was examined on the transmission electron microscopy (TEM, JEM-2010, JEOL, Japan) and scanning electron microscopy (SEM, model JSM-6490, JEOL, Japan). The elemental electronic states and the valence band maximum edge (E_{VB}) of the photocatalysts were determined on the X-ray photoelectron spectroscopy (XPS, Thermo ESCALAB 250, USA). The binding energies were all calibrated to C 1 s peak at 284.6 eV. Fourier transform infrared (FTIR) spectra were obtained on a Nicolet Nexus spectrometer (IRPrestige-21, Shimadzu, Japan). The optical absorption spectra were recorded on a UV–vis spectrophotometer (UV–vis DRS, Shimadzu, Japan) in a diffuse reflectance mode ($BaSO_4$ as reflectance sample), while the photoluminescence (PL) spectra were measured on a fluorescence spectrophotometer (F-7000, Hitachi, Japan). The Electron Paramagnetic Resonance (EPR) measurements were performed on the FLsp920 spectrometer (UK). The Electron Spin Resonance (ESR) signals were recorded on the JES FA200 spectrometer (Japan). The sample was dispersed into a tank of 40 mM DMPO solution before the test under visible light illumination. The O_2 adsorption behaviors on PCN was studied by the temperature programmed chemical adsorption instrument (O_2-TPD, AutoChem1 II 2920, USA). *in situ* DRIFTS analyses followed Dong's work [36], and were performed on the Tensor II FTIR spectrometer (Bruker, German) that equipped with one diffuse-reflectance cell (Harrick, USA) and one sealed reaction chamber.

2.3. Photocatalytic activity evaluation

The photocatalytic performances of the PCN and X-B-PCN in removal of the NO pollutant were evaluated following a published method [4]. Typically, 0.2 g of the sample was dispersed in 10 mL of ethanol by sonication. The resultant suspension was evenly casted onto the bottom of two dishes (made of glass, 12 cm in diameter), which were dried at 60 °C over a heating plate till all the ethanol was evaporated. The two dishes with the photocatalyst film on bottom were then placed in a rectangular reactor (30 × 15 × 10 cm) for reactions. The reactor was then feed with an air flow (flow rate: 2.4 mL min^{-1}) of around 500 ppb NO (C_0). The 300 W halogen lamp (420–700 nm) was used as the visible light source. During reaction, the NO concentration (C) in the outlet flow was recorded. The NO removal efficiency (η) was calculated as

$$\eta\ (\%) = (1 - C/C_0) \times 100\% \quad (1)$$

3. Results and discussion

3.1. Synthesis and characterization of the defective borate-decorated PCN

The dual N defect and borate decoration on PCN were attempted by immersing PCN in a $NaBH_4$ aqueous solution, during which $NaBH_4$ reacts intensively with water to generate Na_3BO_3, H_3BO_3 and H_2 gas:

$$9H_2O\ (l) + 3NaBH_4\ (aq) \rightarrow Na_3BO_3\ (aq) + 2H_3BO_3\ (aq) + 12H_2\ (g) \quad (2)$$

In principal, H_2, as one strong reductive agent, may attack the PCN molecular framework, leading to the fall off of N atoms and then the formation of N defect, while the generated Na_3BO_3 and H_3BO_3 may be adsorbed on PCN via a hydrogen-bond interaction. Fig. 1a presents the XRD patterns of PCN and 1.32-B-PCN, both of which show two characteristic diffraction peaks at around 13.0° and 27.3°, matching with the (100) and (002) crystal plane of PCN [37]. No Na_3BO_3 and H_3BO_3 phase is discerned, possibly due to its low content. The little change in position and intensity of these two peaks in PCN and 1.32-B-PCN suggests that the $NaBH_4$ treatment will not change the overall crystal structure of PCN. Fig. 1b–c compares the TEM images of PCN and 1.32-B-PCN. The PCN displays a typical layered structure with its edge significantly curled. The 1.32-B-PCN keeps the layered structure but its edge appears to be smoothed, which implies that an atomic rearrangement process may occur during $NaBH_4$ treatment. Fig. S1 presents the typical SEM images of the PCN, 0.52-B-PCN, 1.32-B-PCN and 2.64-B-PCN, which further verifies that the X-B-PCN can preserve the layered structure of PCN. However, it also shows that with the X increasing, the sample displays more and more pores on its layers. It suggests that the $NaBH_4$ treatment can indeed etch the atoms from the PCN molecular frameworks, leading to the formation of N defects and the porous structure.

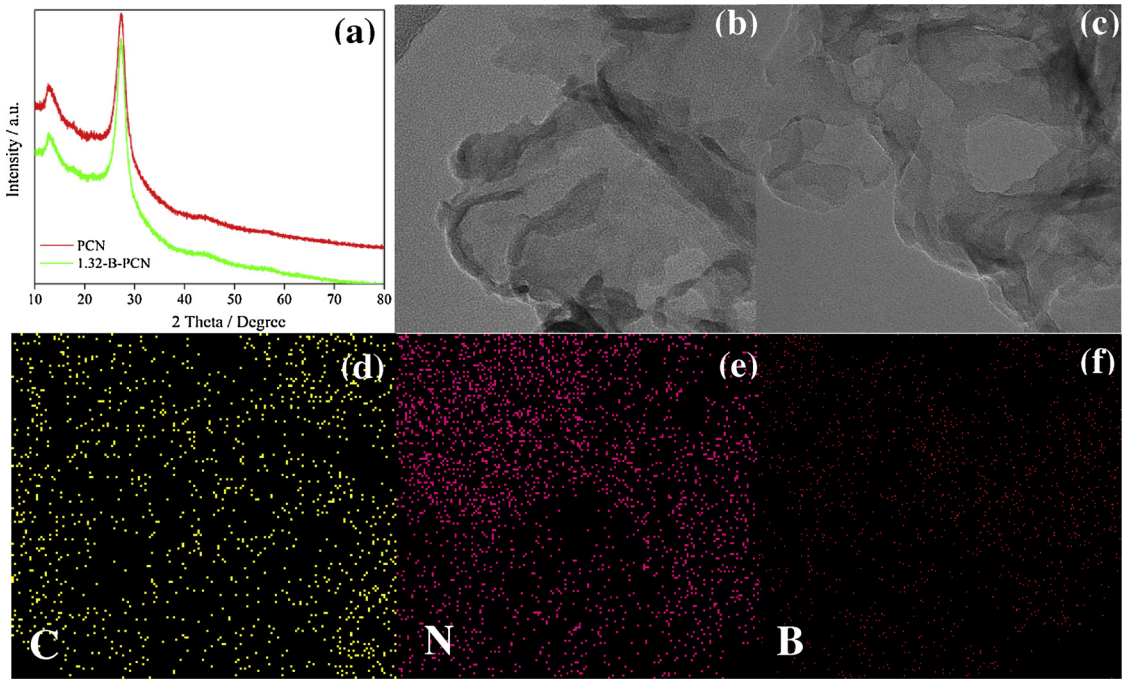

Fig. 1. (a) XRD patterns of PCN and 1.32-B-PCN; TEM images of (b) PCN and (c) 1.32-B-PCN; TEM-EDX elemental mapping of 1.32-B-PCN: (d) C, (e) N and (f) B.

Further nitrogen adsorption-desorption isotherm analyses reveal that the Brunauer-Emmett-Teller (BET) surface area of the sample increase from $46.83\,m^2\,g^{-1}$ of PCN to $53.91\,m^2\,g^{-1}$ of 0.52-B-PCN, $54.86\,m^2\,g^{-1}$ of 1.32-B-PCN and $56.05\,m^2\,g^{-1}$ of 2.64-B-PCN (Fig. S2a). In addition, all the X-B-PCNs own more pores with the diameter ranging from 10 to 40 nm in comparison to the PCN (Fig. S2b). These results are well consistent with the SEM results.

The compositions of PCN and 1.32-B-PCN were examined by the combined techniques of XPS, TEM-EDX elemental mapping and FTIR. The XPS survey scan spectra of PCN and 1.32-B-PCN in Fig. S3 reveal the presence of only C and N in PCN, but extra O, Na and B in 1.32-B-PCN (The B atomic content reaches around 5.4%). Further elemental mapping results in Fig. 1d–f also show that the element C, N and B are uniformly distributed over the layer of 1.32-B-PCN. The high resolution B1 s spectrum in Fig. 2a displays only one peak with a binding energy of 191.9 eV, confirming that B exists in the form of borate [38]. Fig. 2b–d compares the FT-IR spectra of PCN and 1.32-B-PCN. Several new peaks emerge on the spectrum of 1.32-B-PCN at 700, 997, and 1110 cm^{-1}, in comparison to that of PCN. The first two peaks both correspond to the asymmetric stretching vibration of B—O—B bond, while the rest refers to the bending vibration of B—O—B bond [39,40]. The combination of XPS, elemental mapping and FTIR data demonstrate the uniform decoration of borate on PCN after $NaBH_4$ treatment.

The introduction of N defect in PCN by $NaBH_4$ treatment is firstly evidenced by XPS results, where the peak intensity of N-C_3 at 400.2 eV in the high resolution N1 s spectrum of 1.32-B-PCN (in Fig. 3a) is significantly reduced in comparison to that of PCN, and simultaneously, the C/N area ratio of 1.32-B-PCN (0.50) becomes higher than that of PCN (0.47). Further EPR analyses reveal that both PCN and 1.32-B-PCN have a single lorentzian profile with a value of 1.999 [4,20] (See Fig. 3b, obtained under the low temperature and dark condition), which verify the presence of N defect in both PCN and 1.32-B-PCN. The signal of 1.32-B-PCN is stronger than that of PCN, suggestive of a larger number of N defects in 1.32-B-PCN. Furthermore, when the light is turned on, the signal intensities of the two samples are enhanced, implying that these N defects are responsive to the visible light. All the above demonstrate that the facile $NaBH_4$ treatment can introduce the N defects in 1.32-B-PCN.

3.2. Optical property and band structure

As one critical descriptor for photocatalysis, the light absorption behaviors and the band structures of the PCN and X-B-PCN were firstly examined, and the X value was varied to evaluate the effect of N defect and borate decoration. Fig. 4a displays their UV–vis DRS spectra. Interestingly, with a larger X value, the spectrum exhibits an obvious red shift and an enhanced light absorption, but reaches the rightmost at the X of 1.32, and then moves back. Based on these spectra, the band gap (E_g) was determined by the Kubelka–Munk method to decrease from 2.71 eV of PCN to 2.69 eV of 0.52-B-PCN, 2.66 eV of 1.32-B-PCN, and then rebounds to 2.68 eV of 2.64-B-PCN (Fig. S4). The E_{VB} of PCN, 0.52-B-PCN, 1.32-B-PCN and 2.64-B-PCN were measured by VB XPS technique, which lies at 2.28, 2.19, 2.06 and 1.98 eV, respectively (Fig. 4b). According to the formula $E_{CB} = E_{VB} - E_g$, the conduction band minimum edges (E_{CB}) of PCN, 0.52-B-PCN, 1.32-B-PCN and 2.64-B-PCN were then calculated to be -0.43, -0.50, -0.60 and -0.70 eV, respectively. Fig. 4c summarizes the detailed electronic band structures, which clearly shows that the E_{CB} and E_{VB} of X-B-PCN both experience an up-shift with the increase in X. Such an X-dependent optical and band structure feature of PCN should be closely associated with the decorated N defects and borate groups. The introduction of N defect to PCN contributes to the formation of a new energy level above the valence band, which uplifts its valance band edge and narrows the band gap (Fig. 4a–c), allowing the semiconductor to absorb the light of a longer wavelength [41]. And the enhanced light absorption, the reduction in Eg and the up-shift in E_{VB} and E_{CB} with the enlarged X can, therefore, be ascribed to the enriched N defects in the sample treated in a more concentrated $NaBH_4$ solution. The borate decoration will block the active sites of PCN for light absorption and also pose some electronic effect on the band structure of PCN, and mitigate the contribution of N defect, which should be responsible for the moving back of the spectrum when the X crosses 1.32. The more significant left shift with the increased X across 1.32 indicates the increased number of borate group on X-B-PCN after treatment in a more concentrated $NaBH_4$ solution.

PL spectrum is one effective descriptor of the lifetime of the charge carriers in semiconductors, and therefore widely used to evaluate the recombination rate of the photogenerated electron/hole pairs. In basic, a stronger signal of the molecular fluorescence spectrum indicates a

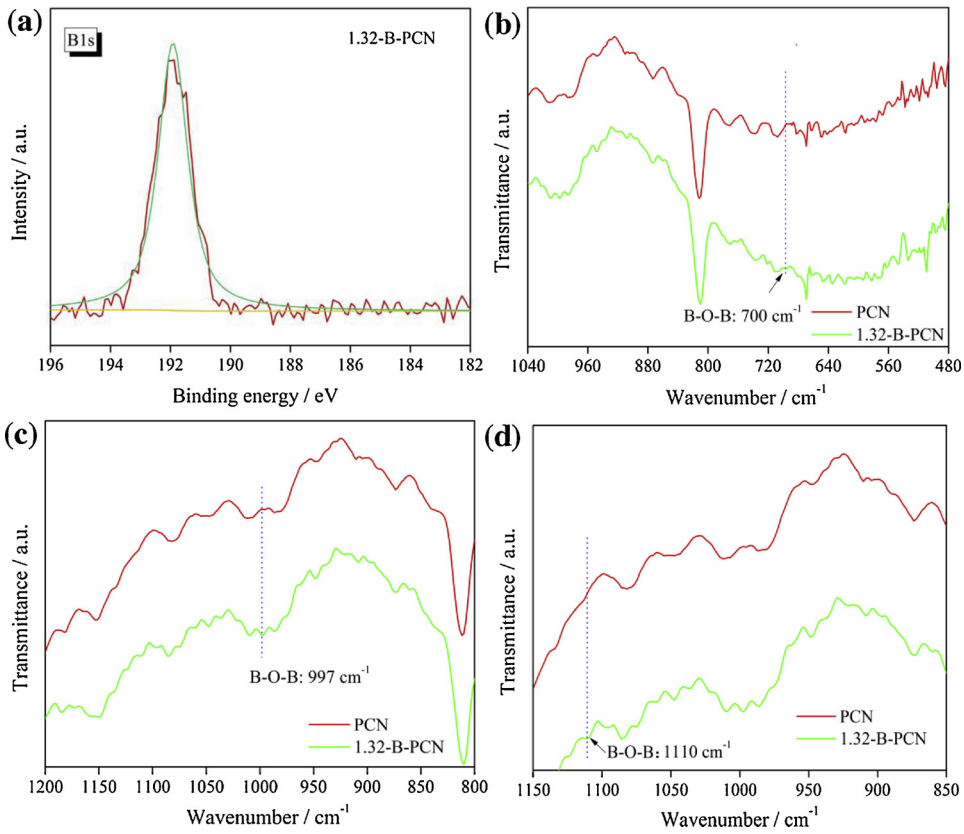

Fig. 2. (a) High resolution B 1 s XPS spectrum of 1.32-B-PCN; (b–d) FT-IR spectra of PCN and 1.32-B-PCN.

larger recombination rate. As shown in Fig. 4d, PCN and all the X-B-PCN display the PL spectra with a peak wavelength at 440–455 nm. Interestingly, with a larger X value, the peak intensity firstly decreases, reaches the lowest at X = 1.32, and then rebounds. The X-dependent variation in the peak intensity should be also associated with the amount of the N defects and borate groups. The N defect can serve to trap the photogenerated electrons, and promote their separation with the hot holes. However, some studies also revealed that the defects might also serve as the active center to accelerate the electron/hole recombination, when its number went over an ideal value (in this work, this value should be reached in 1.32-B-PCN) [42,43]. The presence of borate promotes the reactions of the hot electrons with oxygen, and will thus enhance the separation of the charge carriers [31]. Accordingly, we conclude that both the N defect and borate are enriched on PCN by enlarging the $NaBH_4$ concentration, which is consistent with the results obtained from the UV–vis DRS results. The borate decoration and proper amount of N defects contribute to an enhanced charge carrier separation, while excess N defects pose an adverse effect.

3.3. Photocatalytic performance

The photocatalytic performances of PCN and X-B-PCN with different X values were assessed by their efficiencies in removing the NO pollutant from an air flow under visible light irradiation. The results in Fig. 5a show that all the X-B-PCNs have higher and more stable photocatalytic activities than PCN. The NO removal efficiency versus the X value was then summarized in Fig. 5b. With an increased X, the removal efficiency rises first, reaches the peak at X = 1.32, and then decrease. Such a volcano-like variation trend is well consistent with that of the light absorbance and charge carrier separation efficiency with the X,

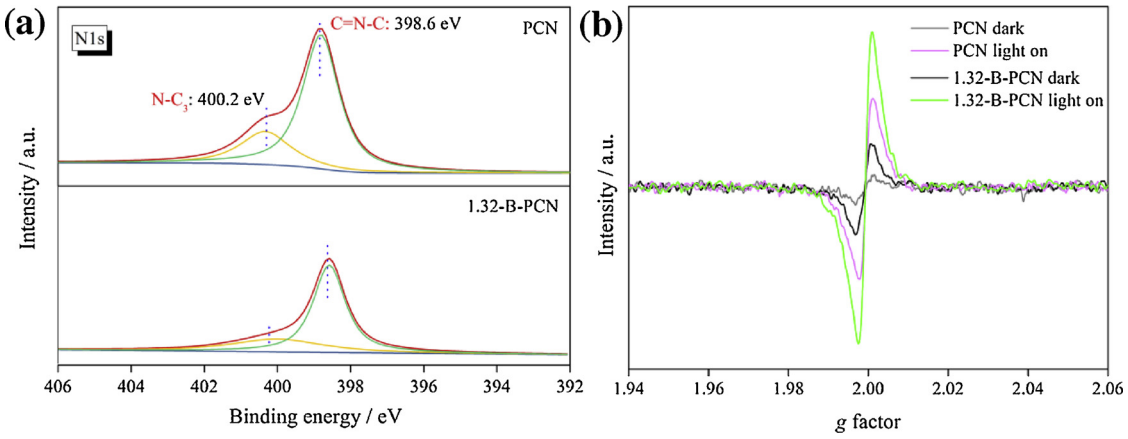

Fig. 3. (a) High resolution N 1 s XPS spectra of PCN and 1.32-B-PCN; (b) EPR spectra of PCN and 1.32-B-PCN.

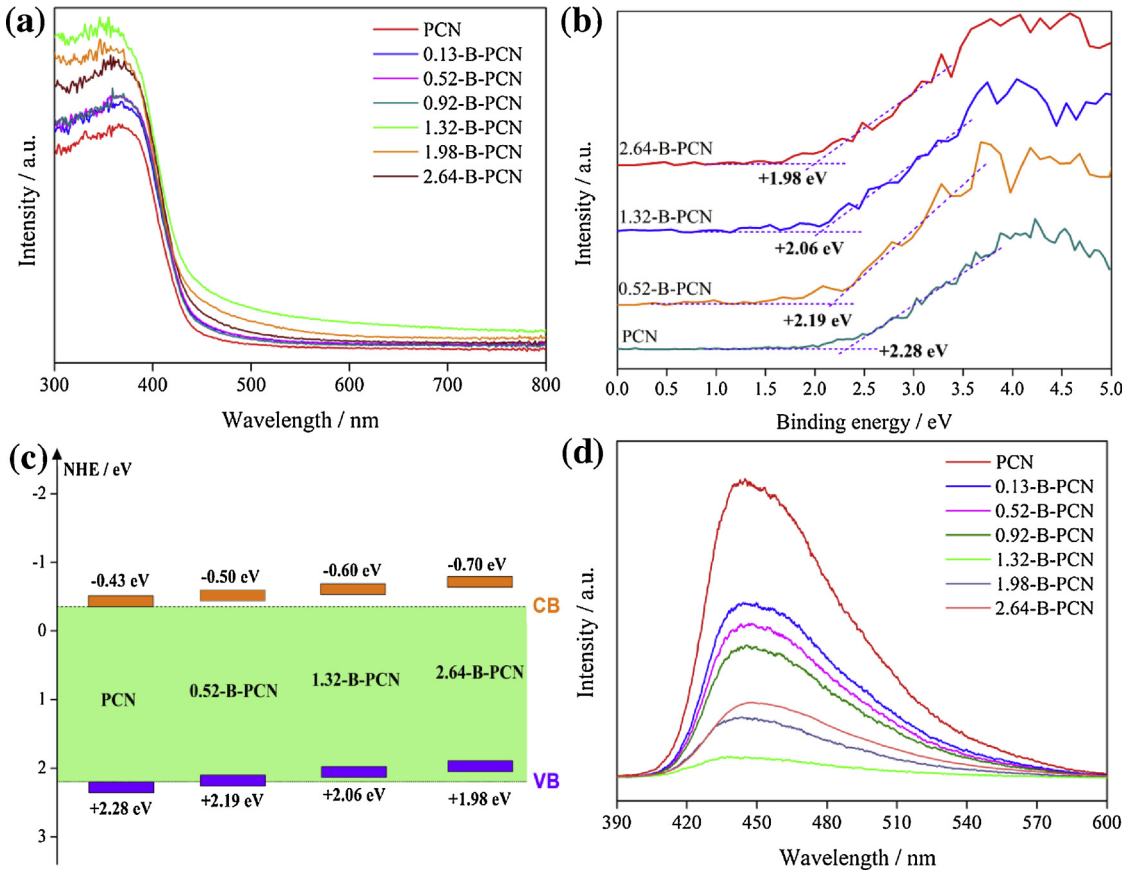

Fig. 4. (a) UV–vis DRS spectra of PCN and X-B-PCN (X = 0.13, 0.52, 0.92, 1.32, 1.98 and 2.64); (b) Determination of the valence band maximum edges (E_{VB}) of PCN and X-B-PCN by VB XPS technique; (c) Illustration of the band structure variation with the X; and (d) PL spectra of the PCN and X-B-PCN (X = 0.13, 0.52, 0.92, 1.32, 1.98 and 2.64).

which clearly reveals the determinant and synergic effect of the N defect and borate decoration on the photocatalytic performance of PCN. Fig. S5 further demonstrates that the modified PCN can preserve its high NO removal efficiency during a repeated test.

Though the above experimental results point to the positive contribution of the synergy of N defect and borate decoration to the photocatalysis, the separated contribution of each one is still unclear. Considering that the borate can be swept by water washing, the 1.32-B-PCN washed with another 50 and 150 mL of water (denoted as 1.32-B-PCN-50 and 1.32-B-PCN-150) were prepared, and their optical properties and photocatalytic performances were then compared with those of PCN and 1.32-B-PCN. The UV–vis DRS spectra in Fig. 6a reveal that the above four photocatalysts follow a weakened light absorbance order of 1.32-B-PCN > 1.32-B-PCN-50 > 1.32-B-PCN-150 > PCN. Fig. 6b shows that with a more sufficient wash, the PL signal rebounds. The weakened light absorbance and electron-hole separation indicate that the borate is indeed swept by sufficient wash, which eliminates its contribution. Fig. 6c compares the photocatalytic performances of the above four samples. 1.32-B-PCN exhibits the highest NO removal efficiency (44.1%), followed by 1.32-B-PCN-50 (40.3%), 1.32-B-PCN-150

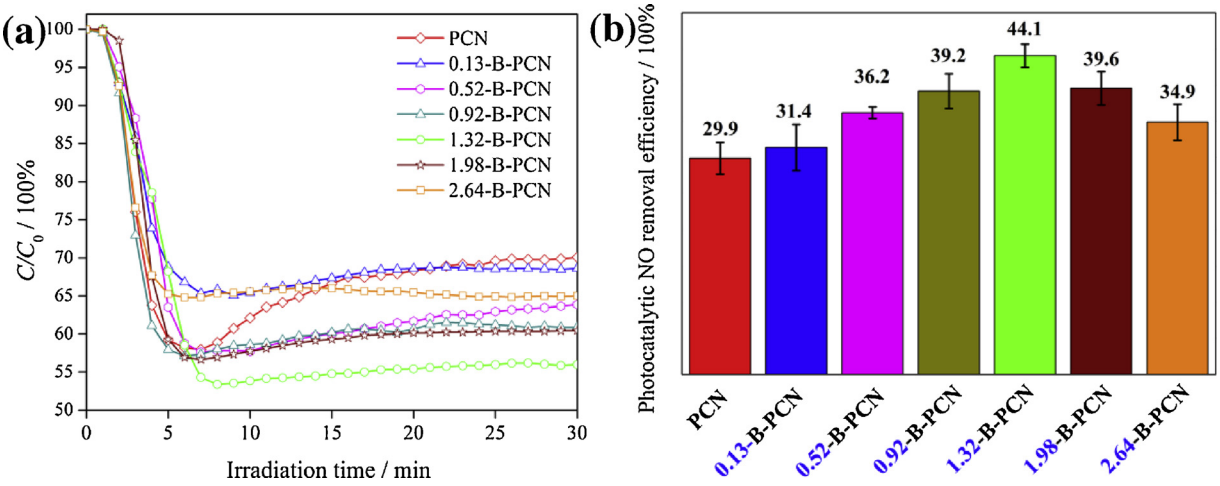

Fig. 5. (a) Photocatalysis activity and (b) the 30-min NO removal efficiency of PCN and X-B-PCN (X = 0.13, 0.52, 0.92, 1.32, 1.98 and 2.64).

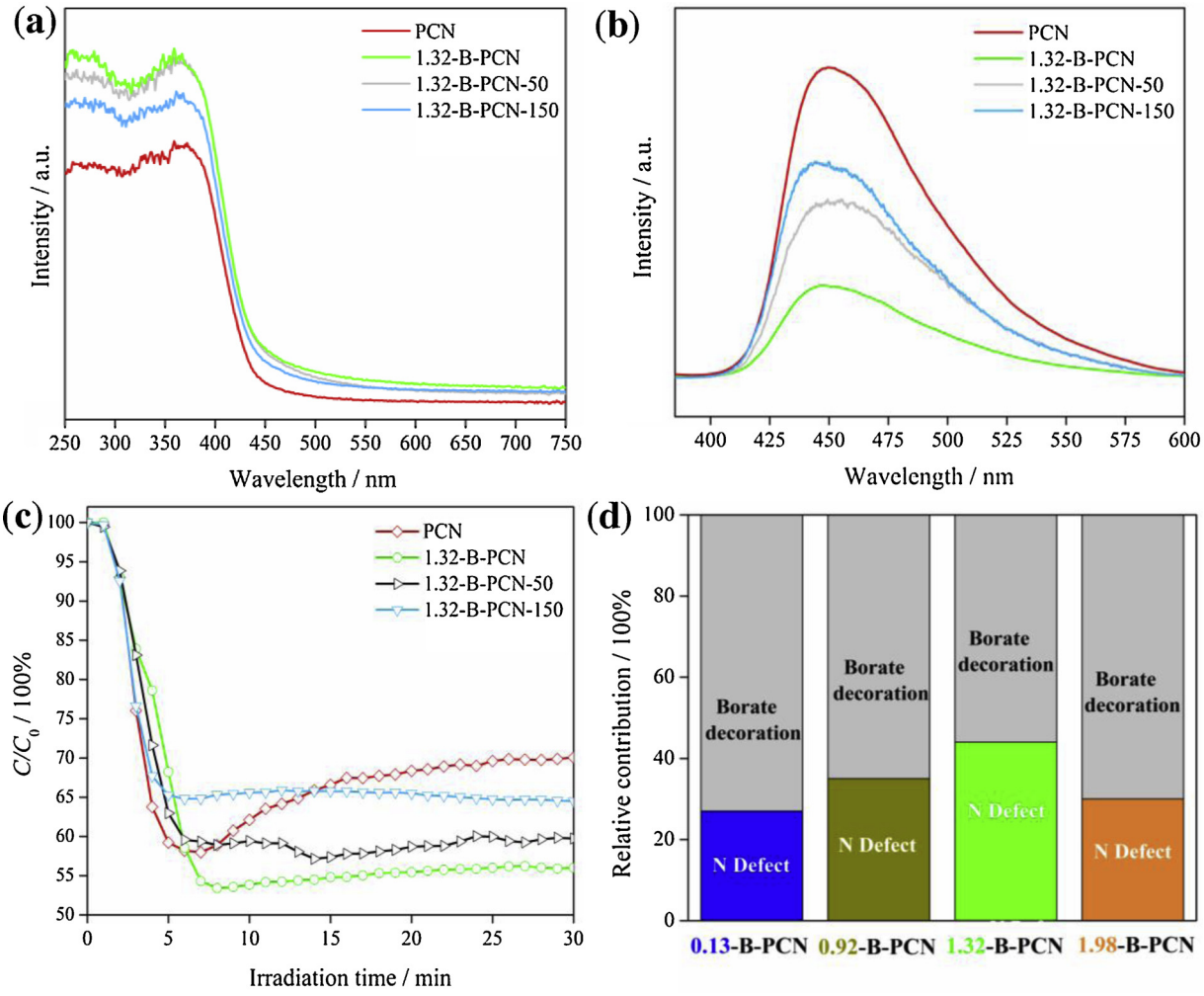

Fig. 6. (a) UV–vis spectra, (b) PL spectra and (c) Photocatalysis activity of PCN and 1.32-B-PCN, 1.32-B-PCN-50, 1.32-B-PCN-150; (d) Relative contribution of the N defect and borate decoration to the photocatalytic activity in 0.13-B-PCN, 0.92-B-PCN, 1.32-B-PCN and 1.98-B-PCN.

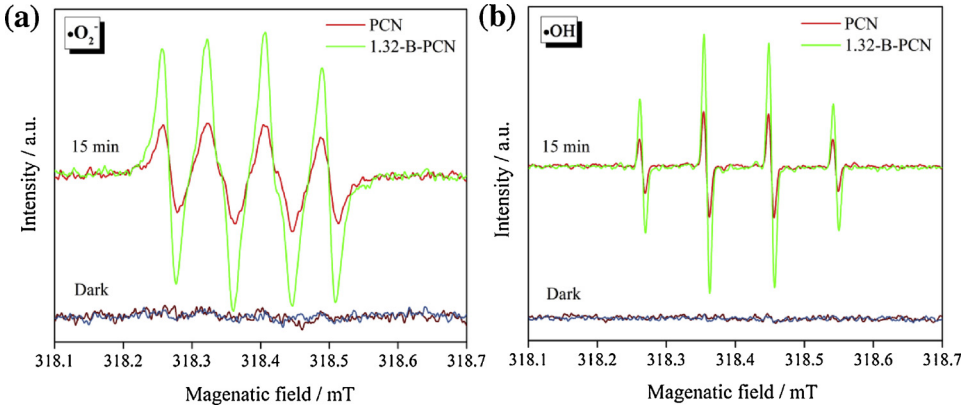

Fig. 7. DMPO spin-trapping ESR spectra of PCN and 1.32-B-PCN: (a) methanol dispersion for DMPO -$^{\cdot}O_2^-$ and (b) aqueous dispersion for DMPO -·OH.

(36.1%), and PCN (29.9%). Assuming that the borate is cleaned up in 1.32-B-PCN-150, its contribution is totally eliminated, and the contribution of N defect can thus be estimated to be 6.2% (36.1% - 29.9%), and that of the borate can be calculated to be 8% (44.1%-36.1%). Accordingly, the contribution proportion of N defect and borate to the photocatalysis of 1.32-B-PCN is 43.6% [6.2% / (6.2% + 8%)] and 56.4% [8% / (6.2% + 8%)], respectively. By the same way, we estimated the contribution proportion in 0.13-B-PCN, 0.92-B-PCN and 2.64-B-PCN, and the results were presented in Fig. 7d. It is interesting to find that the borate decoration contributes more than the defect all the time. With an increased X, the contribution of N defect rises first, reaches the peak at X = 1.32, and then decrease. The rising part demonstrates that the N defect has a positive effect on the photocatalysis, while the descending part reveals that excessive defects contribute negatively to the photocatalysis by accelerating the electron/hole recombination.

3.4. Reaction mechanism

The DMPO-ESR analyses were used to detect the active radicals generated during photocatalysis, and explore more about the synergetic effect of N defect and borate decoration. The $^{\cdot}O_2^-$ and $^{\cdot}OH$ were widely accepted as the two common oxidative radicals, which were both detected in our systems (Fig. 7a–b). However obviously, 1.32-B-PCN produces much more than PCN. For PCN, the redox potential of the photoexcited electrons and holes depends on the band-edge energy of the conduction and valence band of PCN, which lies at -0.43 and + 2.28 eV (Fig. 4c), respectively. The photoexcited electrons and holes are, therefore, energetic enough to reduce the molecular oxygen into $^{\cdot}O_2^-$ (the redox potential for the conversion of O_2 to $^{\cdot}O_2^-$ is −0.33 eV), and oxidize the water to $^{\cdot}OH$ (the redox potential for the conversion of H_2O to $^{\cdot}OH$ is 1.99 eV), respectively. In this case, the enhanced generation of $^{\cdot}O_2^-$ and $^{\cdot}OH$ in X-B-PCN should be attributed to the enhanced light absorbance, the optimized band structure and the improved electron/hole separation under the synergetic effect of N defect and borate decoration.

As revealed by many researches, the acidic group decoration can intensify the O_2 adsorption, and promote the O_2 reaction with the hot electrons to produce more active radicals. To confirm this effect, O_2-TPD on PCN and 1.32-B-PCN were examined in a temperature range of 50–500 °C. The results in Fig. 8a show that both PCN and 1.32-B-PCN display three desorption peaks (peak I, II and III) at their TPD profiles, which indicate that the O_2 is indeed adsorbed on PCN and 1.32-B-PCN. [31] The onset temperature of these three peaks lies at 89.7, 265.7 and 396.8 °C for 1.32-B-PCN, while 89.6, 341.2 and 445.8 °C for PCN, respectively. In general, the desorption at a lower temperature than 100 °C originates from the oxygen physically adsorbed on surface, while at the higher temperature of 200–500 °C, from the oxygen chemically adsorbed on surface. In Fig. 8a, the appearance of two high-temperature desorption peaks in one sample and the difference in the onset desorption temperature in two samples suggest that the oxygen are chemically adsorbed in different sites or manners on PCN and 1.32-B-PCN. The desorption area in TPD profile is closely associated with the amount of oxygen adsorbed on samples [41]. The nearly unchanged area of peak I on PCN and 1.32-B-PCN, and the larger areas of peak II and III on 1.32-B-PCN demonstrate that the borate decoration facilitates the oxygen adsorption on 1.32-B-PCN in a chemical-adsorption manner.

Up to here, we believe that the dual decoration of N defect and borate effectively and synergistically improve the photocatalytic performance of PCN, and the involved mechanism is schematically described in Fig. 8b. The untreated PCN with a band gap of 2.71 eV can absorb the light of a wavelength below 450 nm (Its energy is higher than 2.71 eV), which enables the excitation of electron-hole pairs in PCN with their number depending much on the light intensity. Part of the charge carriers will recombine, while the rest participate in the oxidation of NO. The hot electrons and holes can trigger the generation of highly active radicals $^{\cdot}O_2^-$ and $^{\cdot}OH$ for NO mineralization, while the hot hole can also oxidizes NO in a direct way. However, with the low constitution of the available light (wavelength < 450 nm) in solar light region and the high electron-hole recombination rate in PCN, only a small amount of the charge carriers are available, and thus less oxidative radicals are formed, leading to a lower NO removal efficiency. In X-B-PCN, the presence of N defect allows the PCN to absorb the light with a longer wavelength by optimizing the band structure, and simultaneously promote the electron/hole separation. And the decoration of borate will intensify the O_2 adsorption on PCN, and facilitates its reaction with the hot electrons, leading to an enhanced production of active radicals. With the dual contribution from N defect and borate decoration, the X-B-PCN can absorb more light, and produce more hot charge carriers and oxidative radicals, and eventually present a high photocatalytic activity.

3.5. In-situ DRIFTS study

To gain more insight into the reaction pathway, *in situ* DRIFTS study was performed to track the molecular and chemical bond evolution over 1.32-B-PCN surface during the photocatalytic NO oxidation under a visible light illumination and an oxygen atmosphere. [36] The reaction time-dependent IR spectra were presented in Fig. 9. The baseline was obtained under the helium atmosphere to eliminate the background effect. The 0-min spectrum was recorded after the adsorption-desorption equilibrium of the O_2 and NO. It shows a large number of characteristic peaks at 917, 976, 994, 1009, 1070, 1091, 1139 and 1167 cm^{-1}, which can be all assigned to the bending and stretching vibrations of the adsorbed NO on catalyst [11,44,45]. After turning on the light, the peaks at 994, 1091 and 1139 cm^{-1} disappear completely, while those at 917, 976, 1009, 1070 and 1167 cm^{-1} show a weakened intensity, which indicates that the NO oxidation is in progress. With the running of NO oxidation, some new bands emerge to evidence the formation of nitrate phase. The peaks at 1043, 1057 and 1149 cm^{-1} can be indexed as the stretching vibration of monodentate nitrate (NO_3^-) [35,46], while those at 1022, 1116, 1127 and 1154 cm^{-1} refer to the stretching vibration of the bridging and bidentate nitrate [36]. The formation of the nitrate phase indicates that the NO oxidation is terminated at nitrate. After turning off the light, the intensities of the peaks at 1091, 1139 and 1070 cm^{-1} recover, pointing to re-accumulation of NO, while those at 917 cm^{-1} (N_2O_4) and 1091 cm^{-1} ($N_2O_2^{2-}$) decrease with time, signaling the cease of the reaction. The peaks of nitrate at 926, 976, 1009, 1022, 1043, 1070, 1127 and 1167 cm^{-1}

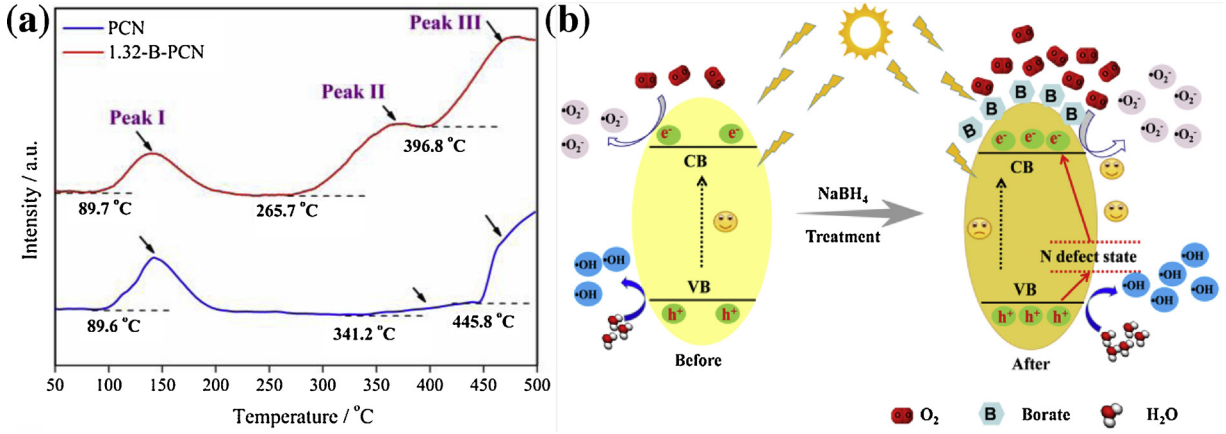

Fig. 8. (a) Corrected profiles of the O_2 temperature-programmed desorption on PCN and 1.32-B-PCN. (b) Schematical description of the synergetic contribution of N defect and borate decoration to photocatalytic performance of PCN.

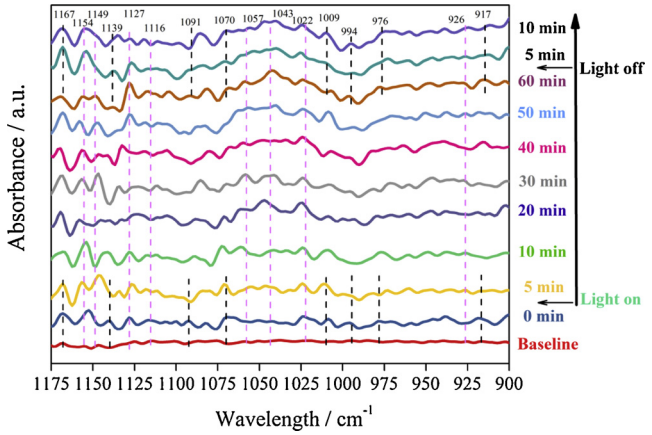

Fig. 9. *In situ* DRIFTS spectra of photocatalytic NO oxidation on 1.32-B-PCN under visible light illumination and an oxygen atmosphere.

preserve well, which is a consequence of the nitrate accumulation on catalyst. Overall, the *in situ* DRIFTS results illustrate the NO pollutant is completely mineralized to nitrate on our defective B-PCN photocatalysts.

4. Conclusions

In conclusion, we developed one cost-effective approach to introduce both the N defects and borate groups on PCN by facilely immersing it in a $NaBH_4$ solution for 15 min, and more importantly, control their number by varying the $NaBH_4$ concentration. Such a well control allows us to make full use of the synergy of N defects and borate to promote light absorbance, charge carrier separation and molecular oxygen adsorption of PCN for an enhanced generation of active $^{\cdot}O_2^-$ and $^{\cdot}OH$ radicals, and an improved photocatalytic activity in NO removal. The reaction pathway study demonstrates that NO is completely mineralized to nitrate. With the facile synthetic method, the high photocatalytic efficiency and the complete mineralization manner, our defective borate-decorated PCN shows highly potential for the scalable application in air pollution remediation.

Acknowledgements

The present work is financially supported by National Natural Science Foundation of China (51878105), Venture & Innovation Support Program for Chongqing Overseas Returnees (cx2017066), the Program for the Top Young Talents of Chongqing, China Postdoctoral Science Foundation (2016M602660), and Chongqing Postdoctoral Science Foundation Funded Project (Xm2016020), Research Startup Foundation of Chongqing Technology and Business University (2016-56-01 and 2016-56-02).

Appendix A. Supplementary data

Supplementary material related to this article can be found, in the online version, at doi:https://doi.org/10.1016/j.apcatb.2019.03.012.

References

[1] G.M. Jiang, K.F. Wang, J.Y. Li, W.Y. Fu, Z.Y. Zhang, G. Johnson, X.S. Lv, Y.X. Zhang, S. Zhang, F. Dong, Electrocatalytic hydrodechlorination of 2,4-dichlorophenol over palladium nanoparticles and its pH-mediated tug-of-war with hydrogen evolution, Chem. Eng. J. 348 (2018) 26–34.
[2] M. Pirhashemi, A. Habibi-Yangjeh, S.R. Pouran, Review on the criteria anticipated for the fabrication of highly efficient ZnO-based visible-light-driven photocatalysts, J. Ind. Eng. Chem. 62 (2018) 1–25.
[3] M. Shekofteh-Gohari, A. Habibi-Yangjeh, M. Abitorabi, A. Rouhi, Magnetically separable nanocomposites based on ZnO and their applications in photocatalytic processes: a review, Crit. Rev. Env. Sci. Technol. 54 (2018) 1–52.
[4] W. Cui, J.Y. Li, F. Dong, Y.J. Sun, G.M. Jiang, W.L. Cen, S.C. Lee, Z.B. Wu, Highly efficient performance and conversion pathway of photocatalytic NO oxidation on SrO-clusters@ amorphous carbon nitride, Environ. Sci. Technol. 51 (2017) 10682–10690.
[5] J. Barrio, M. Shalom, Rational design of carbon nitride materials by supramolecular preorganization of monomers, ChemCatChem 10 (2018) 5573–5586.
[6] J. Barrio, L.H. Lin, P.A. Ochoa, J. Tzadikov, G.M. Peng, J.W. Sun, F. Zamora, X.C. Wang, M. Shalom, Unprecedented centimeter-long carbon nitride needles: synthesis, characterization and applications, Small 14 (2018) 1800633.
[7] L. Shi, F.X. Wang, L. Liang, K.L. Chen, M.S. Liu, R.S. Zhu, J.M. Sun, In site acid template induced facile synthesis of porous graphitic carbon nitride with enhanced visible-light photocatalytic activity, Catal. Commun. 89 (2017) 129–132.
[8] I.F. Teixeira, E.C.M. Barbosa, S.C.E. Tsang, P.H.C. Camargo, Carbon nitrides and metal nanoparticles: from controlled synthesis to design principles for improved photocatalysis, Chem. Soc. Rev. 47 (2018) 7783–7817.
[9] X.J. Wang, W.Y. Yang, F.T. Li, Y.B. Xue, R.H. Liu, Y.J. Hao, In situ microwave-assisted synthesis of porous N-TiO_2/g-C_3N_4 heterojunctions with enhanced visible-Light photocatalytic properties, Ind. Eng. Chem. Res. 52 (2013) 17140–17150.
[10] M. Mousavi, A. Habibi-Yangjeh, S.R. Pouran, Review on magnetically separable graphitic carbon nitride-based nanocomposites as promising visible-light-driven photocatalysts, J. Mater. Sci.-Mater. Electron. 29 (2018) 1719–1747.
[11] G.P. Dong, Y.H. Zhang, Q.W. Pan, J.R. Qiu, A fantastic graphitic carbon nitride (g-C_3N_4) material: Electronic structure, photocatalytic and photoelectronic properties, J. Photochem. Photobiol. C 20 (2014) 33–50.
[12] A. Bafaqeer, M. Tahir, N.A.S. Amin, Well-designed ZnV_2O_6/g-C_3N_4 2D/2D nanosheets heterojunction with faster charges separation via pCN as mediator towards enhanced photocatalytic reduction of CO_2 to fuels, Appl. Catal. B-Environ. 242 (2019) 312–326.
[13] D.L. Jiang, J. Li, C.S. Xing, Z.Y. Zhang, S.C. Meng, M. Chen, Two-dimensional $CaIn_2S_4$/g-C_3N_4 heterojunction nanocomposite with enhanced visible-light photocatalytic activities: interfacial engineering and mechanism insight, ACS Appl. Mater. Interfaces 7 (2015) 19234–19242.
[14] R.R. Hao, G.H. Wang, H. Tang, L.L. Sun, C. Xu, D.Y. Han, Template-free preparation of macro/mesoporous g-C_3N_4/TiO_2 heterojunction photocatalysts with enhanced visible light photocatalytic activity, Appl. Catal. B-Environ. 187 (2016) 47–58.
[15] S. Guo, Z. Deng, M. Li, B. Jiang, C. Tian, Q. Pan, H. Fu, Phosphorus-doped carbon nitride tubes with a layered micro-nanostructure for enhanced visible-light photocatalytic hydrogen evolution, Angew. Chem. Int. Ed. 128 (2016) 1862–1866.
[16] Z. Wang, M. Chen, Y. Huang, X. Shi, Y. Zhang, T. Huang, J. Cao, W. Ho, S. Lee, Self-assembly synthesis of boron-doped graphitic carbon nitride hollow tubes for enhanced photocatalytic NO_x removal under visible light, Appl. Catal. B-Environ. 239 (2018) 352–361.
[17] J. Tzadikov, M. Auinat, J. Barrio, M. Volokh, G. Peng, C. Gervais, Y. Ein-Eli, M. Sholam, Layered boron-nitrogen-carbon-oxygen materials with tunable composition as lithium-ion battery anodes, ChemSusChem 11 (2018) 2912–2920.
[18] G.H. Dong, D.L. Jacobs, L. Zang, C.Y. Wang, Carbon vacancy regulated photoreduction of NO to N_2 over ultrathin g-C_3N_4 nanosheets, Appl. Catal. B-Environ. 218 (2017) 515–524.
[19] Q. Tay, P. Kanhere, C.F. Ng, S. Chen, S. Chakraborty, A.C.H. Huan, T.C. Sum, R. Ahuja, Z. Chen, Defect engineered g-C_3N_4 for efficient visible light photocatalytic hydrogen production, Chem. Mater. 27 (2015) 4930–4933.
[20] W.G. Tu, Y. Xu, J.J. Wang, B.W. Zhang, T.H. Zhou, S.M. Yin, S.Y. Wu, C.M. Li, Y.Z. Huang, Y. Zhou, Z.G. Zou, J. Robertson, M. Kraft, R. Xu, Investigating the role of tunable nitrogen vacancies in graphitic carbon nitride nanosheets for efficient visible-light-driven H_2 Evolution and CO_2 reduction, ACS Sustainable Chem. Eng. 5 (2017) 7260–7268.
[21] C. Liu, C.M. Li, X.D. Fu, F. Raziq, Y. Qu, L.Q. Jing, Synthesis of silicate-bridged ZnO/g-C_3N_4 nanocomposites as efficient photocatalysts and its mechanism, RSC Adv. 5 (2015) 37275–37280.
[22] Y.B. Luan, L.Q. Jing, Y. Xie, X.J. Sun, Y.J. Feng, H.G. Fu, Exceptional photocatalytic activity of 001-facet-exposed TiO_2 mainly depending on enhanced adsorbed oxygen by residual hydrogen fluoride, ACS Catal. 6 (2013) 1378–1385.
[23] H. Park, Y. Park, W. Kim, W. Choi, Surface modification of TiO_2 photocatalyst for environmental applications, J. Photochem. Photobiol. C 15 (2013) 1–20.
[24] D.M. Ruan, S. Kim, M. Fujitsuka, T. Majima, Defects rich g-C_3N_4 with mesoporous structure for efficient photocatalytic H_2 production under visible light irradiation, Appl. Catal. B-Environ. 238 (2018) 638–646.
[25] Z.Y. Liu, X.T. Zhang, S. Nishimoto, T. Murakami, A. Fujishima, Efficient photocatalytic degradation of gaseous acetaldehyde by highly ordered TiO_2 nanotube arrays, Environ. Sci. Technol. 22 (2008) 8547–8551.
[26] W.J. He, Y.J. Sun, G.M. Jiang, Y.H. Li, X.M. Zhang, Y.X. Zhang, Y. Zhou, F. Dong, Defective Bi_4MoO_9/Bi metal core/shell heterostructure: Enhanced visible light photocatalysis and reaction mechanism, Appl. Catal. B-Environ. 239 (2018) 619–627.
[27] J. Ding, W. Xu, H. Wan, D.S. Yuan, C. Chen, L. Wei, G.F. Guan, W.L. Dai, Nitrogen vacancy engineered graphitic C_3N_4-based polymers for photocatalytic oxidation of aromatic alcohols to aldehydes, Appl. Catal. B-Environ. 221 (2018) 626–634.
[28] L.Q. Fang, X.L. Wang, J.J. Zhao, Y.H. Li, Y.L. Wang, X.L. Du, Z.F. He, H.D. Zeng, H.G. Yang, One-step fabrication of porous oxygen-doped g-C_3N_4 with feeble nitrogen vacancies for enhanced photocatalytic performance, Chem. Commun. 52 (2016) 14408–14411.
[29] C. Yue, L.Q. Jing, S. Xin, Y.B. Luan, J.R. Durrant, J.W. Tang, H.G. Fu, Enhanced photocatalytic activity of nc-TiO_2 by promoting photogenerated electrons captured by the adsorbed oxygen, Phys. Chem. Chem. Phys. 14 (2012) 8530–8536.
[30] D.N. Liu, L.Q. Jing, P. Luan, J.W. Tang, H.H. Fu, Enhancement effects of cobalt phosphate modification on activity for photoelectrochemical water oxidation of

TiO_2 and mechanism insights, ACS Appl. Mater. Interfaces 5 (2013) 4046–4052.
[31] C. Liu, L.Q. Jing, L.M. He, Y.B. Luan, C.M. Li, Phosphate-modified graphitic C_3N_4 as efficient photocatalyst for degrading colorless pollutants by promoting O_2 adsorption, Chem. Commun. 50 (2014) 1999–2001.
[32] J. Barrio, A. Grafmuller, J. Tzadikov, M. Shalom, Halogen-hydrogen bonds: a general synthetic approach for highly photoactive carbon nitride with tunable properties, Appl. Catal. B-Environ. 235 (2018) 681–688.
[33] Y.Z. Hong, C.S. Li, D. Li, Z.Y. Fang, B.F. Luo, X. Yan, H.Q. Shen, B.D. Mao, W.D. Shi, Precisely tunable thickness of graphitic carbon nitride nanosheets for visible-light-driven photocatalytic hydrogen evolution, Nanoscale 9 (2017) 14103–14110.
[34] L.Q. Jing, J. Zhou, J.R. Durrant, J.W. Tang, D.N. Liu, H.G. Fu, Dynamics of photogenerated charges in the phosphate modified TiO_2 and the enhanced activity for photoelectrochemical water splitting, Energy Environ. Sci. 5 (2012) 6552–6558.
[35] G.H. Dong, W.K. Ho, C.Y. Wang, Selective photocatalytic N_2 fixation dependent on g-C_3N_4 induced by nitrogen vacancies, J. Mater. Chem. A 3 (2015) 23435–23441.
[36] G.M. Jiang, X.W. Li, M.N. Lan, T. Shen, X.S. Lv, F. Dong, S. Zhang, Monodisperse bismuth nanoparticles decorated graphitic carbon nitride: enhanced visible-light-response photocatalytic NO removal and reaction pathway, Appl. Catal. B-Environ. 205 (2017) 532–540.
[37] F. Dong, Z.W. Zhao, T. Xiong, Z.L. Ni, W.D. Zhang, Y.J. Sun, W.K. Ho, In situ construction of g-C_3N_4/g-C_3N_4 metal-free heterojunction for enhanced visible-light photocatalysis, ACS Appl. Mater. Interfaces 5 (2013) 11392–11401.
[38] S.C. Yan, Z.S. Li, Z.G. Zou, Photodegradation of rhodamine B and methyl orange over boron-doped g-C_3N_4 under visible light irradiation, Langmuir 26 (2010) 3894–3901.
[39] P. Pascuta, L. Pop, S. Rada, M. Bosca, E. Culea, The local structure of bismuth borate gluropium ions evidenced by FT-IR spectroscopy, J. Mater. Sci.-Mater. EL 19 (2008) 424–428.
[40] H.Q. Dai, J. Gong, H. Kim, D. Lee, A novel method for preparing ultra-fine alumina-borate oxide fibres via an electrospinning technique, Nanotechnology 13 (2002) 674–677.
[41] P. Niu, G. Liu, H.M. Cheng, Nitrogen vacancy-promoted photocatalytic activity of graphitic carbon nitride, J. Phys. Chem. C 116 (2012) 11013–11018.
[42] X.C. Jiao, Z.W. Chen, X.D. Li, Y.F. Sun, S. Gao, W.S. Yan, C.M. Wang, Q. Zhang, Y. Lin, Y. Luo, Y. Xie, Defect-mediated electron–hole separation in one-unit-cell $ZnIn_2S_4$ layers for boosted solar-driven CO_2 reduction, J. Am. Chem. Soc. 139 (2017) 7586–7594.
[43] M. Kong, Y.Z. Li, X. Chen, T.T. Tian, P.F. Fang, F. Zheng, X.J. Zhao, Tuning the relative concentration ratio of bulk defects to surface defects in TiO_2 nanocrystals leads to high photocatalytic efficiency, J. Am. Chem. Soc. 133 (2011) 16414–16417.
[44] L. Sivachandiran, F. Thevenet, A. Rousseau, D. Bianchi, NO_2 adsorption mechanism on TiO_2: an in-situ transmission infrared spectroscopy study, Appl. Catal. B-Environ. 198 (2016) 411–419.
[45] T. Weingand, S. Kuba, K. Hadjiivanov, H. Knözinger, Nature and reactivity of the surface species formed after NO adsorption and NO + O_2 coadsorption on a WO_3–ZrO_2 Catalyst, J. Catal. 209 (2002) 539–546.
[46] X.W. Li, W.D. Zhang, W. Cui, Y.J. Sun, G.M. Jiang, Y.X. Zhang, H.W. Huang, F. Dong, Bismuth spheres assembled on graphene oxide: Directional charge transfer enhances plasmonic photocatalysis and in situ DRIFTS studies, Appl. Catal. B-Environ. 221 (2018) 482–489.